Published in final edited form as:
Nat Immunol. 2018 August ; 19(8): 859–870. doi:10.1038/s41590-018-0161-8.

Epithelial damage and tissue γδ T cells promote a unique tumor-protective IgE response

Greg Crawford[1], **Mark David Hayes**[1], **Rocio Castro Seoane**[1], **Sophie Ward**[1], **Tim Dalessandri**[1], **Chester Lai**[2], **Eugene Healy**[2], **David Kipling**[3], **Charlotte Proby**[4], **Colin Moyes**[5], **Kile Green**[6], **Katie Best**[6,7], **Muzlifah Haniffa**[6,7], **Marina Botto**[1], **Deborah Dunn-Walters**[8], and **Jessica Strid**[1,*]

[1]Department of Medicine, Imperial College London, London, UK

[2]Dermatopharmacology, Clinical and Experimental Sciences, Faculty of Medicine, University of Southampton, Southampton, United Kingdom; Dermatology, University Hospital Southampton NHS Foundation Trust, Southampton, United Kingdom

[3]Division of Cancer and Genetics, School of Medicine, Cardiff University, Cardiff, UK

[4]Division of Cancer Research, School of Medicine, University of Dundee, Ninewells Hospital & Medical School, Dundee, UK

[5]Department of Pathology, Greater Glasgow and Clyde NHS, Queen Elizabeth University Hospital, Glasgow, UK

[6]Institute of Cellular Medicine, Newcastle University, Newcastle upon Tyne, UK

[7]Department of Dermatology and Newcastle Biomedical Research Centre, Royal Victoria Infirmary, Newcastle Hospitals NHS Foundation Trust, Newcastle upon Tyne, UK

[8]Faculty of Health and Medical Sciences, School of Biosciences and Medicine, University of Surrey, Guildford, Surrey, UK

Abstract

Corresponding author: Jessica Strid, Department of Medicine, Imperial College London, London, W12 0NN, UK; Tel: +44 (0) 20 3313 1475; Fax: +44 (0) 20 3313 2379; j.strid@imperial.ac.uk.

Data availability

The data supporting the findings of this study are available from the corresponding author upon request. RNA sequencing data is available from the public repository on the National Center for Biotechnology Information's Sequence Read Archive in raw format (BioProject: PRJNA417372; BioSample accession: SAMN07985450, SAMN07985451, SAMN07985452, SAMN07985453, SAMN07985454, SAMN07985455).

Author contributions

G.C. performed and analyzed the experiments with help from M.D.H., R.C.R., S.W. and T.D. C.L. and E.H. provided human blood and SSC samples for FACS. C.P. and C.M. provided and graded human skin and tumor samples for Nanostring. M.H. and K.B. generated SCC NanoString data and K.G. analyzed it. D.K. assisted with sequencing analysis and D.D-W. with sequencing analysis and interpretation. M.B. assisted with data interpretation and manuscript preparation. J.S. performed and analyzed some experiments, directed the study and wrote the manuscript.

Competing financial interest statement

The authors declare no competing financial interests.

Europe PMC Funders Author Manuscripts

IgE is an ancient and conserved immunoglobulin isotype with potent immune function. Nevertheless, the regulation of IgE responses remains enigmatic and evidence for a role of IgE in host defense is limited. Herein we describe that topical exposure to a common environmental DNA-damaging xenobiotic initiated stress-surveillance by γδTCR$^+$ intraepithelial lymphocytes resulting in class-switching to IgE in B cells and accumulation of autoreactive IgE. High-throughput antibody sequencing revealed that γδ T cells shaped the IgE repertoire by supporting specific VDJ rearrangements with unique CDRH3 characteristics. This endogenous IgE response, via the FcεRI, protected against epithelial carcinogenesis and *FceR1a* expression in human squamous cell carcinoma correlated with good disease prognosis. This data indicate a joint role for T and B cell immune-surveillance in epithelial tissues and suggests that IgE is part of the host defense against epithelial damage and tumor development.

IgE is an ancient and highly conserved immunoglobulin isotype found in all mammals1. It is thought that IgE has evolved to provide protection against infection by macroparasites, such as helminths. However, although IgE is elevated in both mice and humans with helminth infections, IgE is not critical for protective immunity against helminths and much of the IgE raised is not parasite-specific2. An alternative hypothesis suggests that IgE is important for immune responses against environmental toxins such as venoms3, and indeed, recent data indicates that IgE can protect against bee venom and limit snake venom toxicity4, 5, 6. Furthermore, aberrant IgE responses causing allergies are frequently directed at environmental irritants and non-replicating agents. A role for IgE in defending against immediate danger would be consistent with the very rapid mobilization of its effector functions. Therefore a broader paradigm proposes that IgE represents an arm of early immune host-defense against xenobiotics or large parasites threatening tissue integrity7. However, what drives these IgE responses *in vivo*, what they recognize and whether they play a wider role in immune defense remain unknown.

IgE responses occur most frequently in epithelial tissues such as the skin, lung and gut, which contain resident IgE-binding cells. These barrier surfaces are continuously exposed to challenges from environmental xenobiotics and a prominent feature of their response to external insults is induction of type 2 immunity8 and IgE9, 10. In the murine skin epithelia, a resident γδTCR$^+$ population of intraepithelial lymphocytes (IEL) controls tissue homeostasis via induction of IL-1311, a type 2 cytokine, and also promotes IgE upon challenge with protein allergens on stressed tissue12. These IELs can directly sense epithelial cell dysregulation via stress-sensing receptors, such as NKG2D, and this pathway plays a key role in promoting the IgE response12, 13. The capacity of IELs to detect epithelial cell stress and initiate a restorative response has been termed lymphoid stress-surveillance and plays an important role in early detection of stressed and pre-malignant cells13. Indeed, tissue-specific IELs regulate epithelial tissue integrity and are key to host-protection against carcinogenesis11, 13.

Many toxins and xenobiotics are also carcinogens. Hence, in defending against environmental xenobiotics, IgE may simultaneously confer protection against transformation and cancer in exposed tissues. Here we report the development of a potent and dominant IgE response following topical exposure to the common environmental xenobiotic and

carcinogen, 7,12-dimethylbenz[a]anthracene (DMBA). This endogenous IgE response was autoreactive and was required for protection against cutaneous carcinogenesis. Further, we show that tissue-resident $\gamma\delta TCR^+$ IELs had a unique role in initiating and regulating IgE production, driving an early, innate-like response, which directed a subsequent adaptive response supported by IL-4-producing $CD4^+$ αβ T cells. Deep-sequencing of IgE and IgG1 from germinal center (GC) B cells and plasma cells (PCs) indicated that $\gamma\delta TCR^+$ IELs shaped a distinct IgE repertoire that was dependent on the presence of DNA-damage in epithelial cells. Thus, lymphoid stress-surveillance promoted a unique IgE response, which was part of an early host defense mechanism providing protection against cancer.

Results

Carcinogen-induced epithelial cell damage triggers IgE responses

DNA-damaging xenobiotics such as DMBA are commonly found in the environment and have been implicated in carcinogenesis14, 15. We found that a single topical application of DMBA to the back skin of wild-type mice induced an IgE response in serum within 4 days (Fig. 1a). DMBA exposure was associated with upregulation of the NKG2D-ligand Rae-1 on skin epithelial cells (Supplementary Fig. 1a), indicating epithelial cell stress. The number of epithelial cells containing double-stranded (ds) DNA-breaks, assessed by staining for the phosphorylated histone H2A variant H2AX (γH2AX), peaked between 3-7 days after DMBA exposure (Supplementary Fig. 1b,c). Epidermal Langerhans cells (LCs) must metabolize DMBA to the more mutagenic compound DMBA-trans-3,4-dihydrodio to cause substantial DNA-damage. Langerin-DTA mice, which do not have LCs, showed less epithelial cell DNA-damage following a single dose of DMBA16 (Supplementary Fig. 1d) and failed to show increased serum IgE compared to non-transgenic littermate controls (NLC) (Fig. 1b). However, Langerin-DTA mice generated IgE to other topical challenges12 and, if exposed to DMBA repeatedly, they developed both DNA-damage *and* IgE responses (Supplementary Fig. 1d,e). Other DNA-damaging skin challenges such as UV-irradiation also induced IgE (Supplementary Fig 1f,g). Once weekly exposure to DMBA led to the development of papillomas and squamous cell carcinomas (SCCs) after 8-15 weeks. This was associated with high amounts of serum IgE, which rose progressively as epithelial DNA-damage accumulated (Fig. 1c). When DMBA was given daily for 5 days only, mice developed skin tumors and serum IgE showed a progressive rise during 12 weeks (Supplementary Fig. 1h). The systemic IgE responses were paralleled by infiltration and accumulation of IgE in acutely damaged skin (Fig. 1d) and in skin tumors (Fig. 1d,e). The tissue IgE was mainly carried by FcεRI-expressing basophils (Fig. 1d). More mature IgE transcripts were expressed in the tumor tissue than the adjacent skin, indicating some local IgE production, whereas IgG1 and IgM transcripts were lower in tumors than adjacent skin (Fig. 1f). This data indicate that the epithelial cell damage triggered by DMBA exposure potently promoted IgE production which accumulated in the resulting skin tumors.

Topical carcinogen exposure induces local B cell class-switching

To investigate the origin of the DMBA-induced IgE response, we examined B cells in the skin-draining LNs during acute DMBA exposure (pre-malignancy). Two applications of DMBA, 3 days apart, on the ear skin induced enlarged skin-draining LNs with formation of

GCs and class-switching of GC B cells (Fig. 2a) as well as increased numbers of $CD138^+$ PCs, which had class-switched primarily to IgE and IgG1, with little or no induction of IgG2a (Fig. 2b). There was no induction of GCs or class-switched PCs in the spleen (data not shown), suggesting the response was localized to the skin-draining LNs. Weekly exposures to DMBA on back skin for 5 weeks also induced GCs and IgE^+ and $IgG1^+$ PCs. However, under these conditions, the GC structures and the $IgG1^+$ PCs diminished from week 3, resulting in a dominant IgE response (Fig. 2c). By week 5 post-exposure, nearly 80% of all $CD138^+$ PCs in the LNs had switched to IgE (Fig. 2c). Thus, skin exposure to DMBA promotes a local type 2 B cell response with dominant and prevailing IgE production.

Carcinogen-induced IgE protects against carcinogenesis

To explore whether the IgE response induced by DMBA was important for host defense, we assessed skin tumor formation in *Igh7*$^{-/-}$ mice, which lack IgE. Following once weekly DMBA exposure *Igh7*$^{-/-}$ mice developed tumors sooner and more rapidly, as well as significantly more and larger tumors than their wild-type counterparts (Fig. 3a). The IgG1 response in the DMBA-treated *Igh7*$^{-/-}$ mice was identical to wild-type mice (Supplementary Fig. 2a). In addition, the number of IgE-effector cells in the tissue was similar to wild-type (Supplementary Figure 3a). *FceR1a*$^{-/-}$ mice, which lack the high affinity receptor for IgE, also had enhanced susceptibility to DMBA carcinogenesis compared to wild-type (Fig 3b), despite having similar IgE and IgG1 amounts in serum (Supplementary Fig 2b), suggesting the protective effect of IgE was mediated by signaling through FcεRI. $CD45^{lo}cKit^-Fc\varepsilon RI^+$ basophils represented the main IgE^+ cell population in the tumors (Fig. 1d). *Cpa3*$^{Cre/+}$ mice, which have Cre-recombinase inserted in the Cpa3 locus, and lack skin mast cells, showed similar susceptibility to tumor development as *Cpa3*$^{+/+}$ littermates following DMBA carcinogenesis, suggesting that, most likely, $Fc\varepsilon RI^+$ basophils mediated the protection against carcinogenesis (Supplementary Fig. 3b). Splenic $CD45^{lo}cKit^-CD41^+Fc\varepsilon RI^+$ basophils from *Igh7*$^{-/-}$ mice produced IL-4 and IL-6 and degranulated equivalent to basophils from wild-type spleens upon PMA/ionomycin stimulation, however the skin tumour cytokine microenvironment was significantly altered in *Igh7*$^{-/-}$ mice compared to wild-type (Supplementary Fig. 3c-e).

To investigate whether similar IgE responses occur in humans, we analyzed newly incised skin SSC samples from 12 patients. $Fc\varepsilon RI^+$ cells were found in all tumor and peri-lesional skin samples, varying in frequency from around 1% to over 40% of the tumor infiltrating $CD45^+$ leukocytes (Fig. 3c). The $Fc\varepsilon RI^+$ cells were mainly found in the peritumoral infiltrate at the interface between the stroma and the neoplastic keratinocytes with some entering the tumor and/or hair follicle (averaging 11.7±2.9 cells per mm^2) (Supplementary Fig. 4). $Fc\varepsilon RI^+$ cells accumulated more in the skin compared to matched blood samples, however, tumor tissue contained fewer $Fc\varepsilon RI^+$ cells than histopathologically healthy peri-lesional skin from the same patient (Fig. 3c). In an additional cohort of 56 SCC patients, gene-expression analysis revealed that expression of *FceR1a* mRNA was higher in unaffected skin areas than in developed tumors, with the lowest expression of *FceR1a* mRNA detected in high-risk and metastatic SCCs (Fig. 3d). A significant linear trend was observed between *FceR1a* mRNA expression and the risk for more advanced SSC (Fig. 3d).

Together these data indicate that IgE, via FcεRI, protected against DMBA-induced SCC and that fewer FcεRI-expressing leukocytes in human SSC correlates with risk of more severe disease.

Carcinogen-induced humoral immunity depends on αβ T cell-derived IL-4

Conventional and non-conventional modes of inducing class-switching to IgE have been described8. We first explored whether induction of tumor-protective IgE was dependent on αβ T cells. *Tcrb*$^{-/-}$ mice, which lack αβ T cells, had no enlargement of skin-draining LNs, no GCs, and no IgG1^{+} or IgE^{+} PCs following twice topical DMBA to the ear skin compared to wild-type mice (Fig. 4a). The response was restored by transferring polyclonal CD4^{+} T cells, but not TCR-restricted transgenic OTII CD4^{+} T cells in *Tcrb*$^{-/-}$ mice (Supplementary Fig. 5a), indicating it was dependent on a normal TCR repertoire. Furthermore, injection of α-CD40L blocking antibody partially inhibited LN enlargement and repressed GC formation and generation of IgE^{+} and IgG1^{+} PCs in wild-type mice (Supplementary Fig. 5b). Similar defects in class-switching to IgE^{+} and IgG1^{+} PCs were seen *Il4*$^{-/-}$ mice, which cannot produce IL-4, although *Il4*$^{-/-}$ mice showed an enlargement of LNs comparable to wild-type mice and had some GC B cells (Fig. 4a). *Il4*$^{-/-}$ mice had some class-switching to IgG2a, which was never observed in wild-type or in *Tcrb*$^{-/-}$ mice (data not shown). Wild-type→*Il4*$^{-/-}$ BM chimeras induced IgE^{+} and IgG1^{+} PCs comparably to wild-type→wild-type chimeras following topical DMBA treatment, whereas *Il4*$^{-/-}$→wild-type chimeras induced significantly less IgE^{+} and IgG1^{+} PCs (Supplementary Fig. 5c), indicating IL-4 was derived from haemapoeitic cells, and not irradiation-resistant skin-resident cells. To test whether the requirement for αβ T cell for IgE/IgG1 class-switching reflected a need for IL-4, we reconstituted *Tcrb*$^{-/-}$ mice with wild-type or *Il4*$^{-/-}$ CD4^{+} T cells 24hr prior to DMBA exposure. Only the wild-type CD4^{+} αβ T cells were able to rescue the GC response and IgG1/IgE production in the skin-draining LN of the reconstituted *Tcrb*$^{-/-}$ mice (Fig. 4b). Moreover, *Il4*$^{-/-}$ mice showed significantly earlier onset, higher incidence of tumors and larger tumors compared to wild-type controls following weekly DMBA treatment (Fig. 4c), indicating that IL-4 was required for tumor protection. Tumor-bearing *Il4*$^{-/-}$ mice did not produce IgE and had diminished production of IgG1, but higher IgG2a, in serum compared to wild-type (Supplementary Fig. 2c). Thus, αβ T cell-derived IL-4 is critical for IgE production and tumor protection following DMBA exposure.

Induction of tumor-protective IgE requires γδ TCR^{+} IEL

Skin γδTCR^{+} IELs are key for protective immunity against chemical carcinogenesis and are strong inducers of local type 2 immune responses11, 12, 13. We found that *Tcrd*$^{-/-}$ mice, which lack γδ T cells, had less LN hypertrophy following topical DMBA exposure to the ear skin, but normal numbers of GC B cells compared to wild-type mice (Fig. 5a). *Tcrd*$^{-/-}$ mice developed comparable IgG1^{+} PCs, but had significantly impaired IgE PC responses compared to wild-type mice (Fig. 5a). The reduction in IgE was already detected at day 4, a time-point when the numbers of IgE^{+} PCs and serum IgE were increased in wild-type mice, but remained undetectable in *Tcrd*$^{-/-}$ mice (Fig. 5a,b). GCs were not yet enlarged in wild-type mice at day 4 (Fig. 5a), suggesting that the γδ T cell-dependent IgE response at this time may be of extra-follicular origin. To explore this, we utilized CD19^{cre}Bcl-6$^{fl/fl}$ mice, which have a B cell-specific defect in the transcription factor Bcl-6. CD19^{cre}Bcl-6$^{fl/fl}$ mice

did not develop a GC response following topical DMBA application, despite LN enlargement, but the number of IgE^+ and $IgG1^+$ PCs in the LN were equivalent to in Bcl-6 heterozygous littermates and wild-type mice (Supplementary Fig. 5d). We next asked whether the γδ T cells involved in the response were located in the skin itself or in a secondary lymphoid organ such as the draining-LNs. Skin resident $\gamma\delta TCR^+$ IELs are radiation-resistant11 and in *Tcrd*$^{-/-}$→wild-type and wild-type→*Tcrd*$^{-/-}$ BM chimeras γδ T cells were detected only in the skin or LNs respectively (Fig. 5c). When these chimeras were treated topically with DMBA, IgE was significantly reduced only in wild-type→*Tcrd*$^{-/-}$ chimeras, in which $\gamma\delta TCR^+$ IELs were missing from the skin, but γδ T cells were present in the LNs, compared to wild-type chimeric controls (Fig. 5d). The number of $IgG1^+$ PCs was similar in *Tcrd*$^{-/-}$→wild-type, wild-type→*Tcrd*$^{-/-}$ and control chimeras (Fig. 5d). The $V\gamma4^+$ and other 'non-$V\gamma5^+$' γδ T cells in the skin of *Tcrd*$^{-/-}$→wild-type, wild-type→*Tcrd*$^{-/-}$ chimeras were similar to wild-type chimeric controls (Fig. 5c). In addition, *Vg5Vd1*$^{-/-}$ mice, which lack only the canonical $V\gamma5V\delta1^+$ IELs, had fewer IgE^+ PCs following topical DMBA treatment compared to wild-type mice (Fig. 5e), suggesting that $V\gamma5^+$ IELs were most likely the IgE-promoting γδ T cell subset. These observations indicate that DMBA-induced IgE depended on $\gamma\delta TCR^+$ IEL in the tissue.

γδ T cells promote a distinct IgE repertoire in response to carcinogen

To understand the nature of the humoral response produced during epithelial cell damage, and the role of γδ T cell immune-surveillance, we sorted $B220^+CD95^+GL7^+$ GC B cells and $FSC^{hi}CD95^{hi}CD138^+$ PCs from the skin draining LNs of wild-type and *Tcrd*$^{-/-}$ mice 7 days after the last of two topical DMBA exposures. Analysis of the IgG1 and IgE heavy-chain repertoires using high-throughput sequencing revealed that IgE-producing clones had the largest clone expansion in wild-type mice (Supplementary Fig. 6a). As expected, the average clone sizes for IgG1 were greater amongst PCs than GC B cells (Fig. 6a). In contrast, IgE clones among PCs and GC B cells were equivalent and were larger than IgG1 clones (Fig. 6a). Furthermore, *Tcrd*$^{-/-}$ mice had defective IgE clone expansion in GC B cells compared to wild-type, while IgG1 clone expansion was similar (Fig. 6b). Alakazam tool17, an analysis framework for adaptive immune-receptor repertoire sequencing, indicated that the IgE^+ PC repertoire was significantly less diverse in *Tcrd*$^{-/-}$ compared with wild-type mice in all but the most common clones (Fig. 6c). In contrast, the $IgG1^+$ PC repertoire diversity in *Tcrd*$^{-/-}$ mice was similar to wild-type (Fig. 6c).

We also analyzed the physicochemical properties of the CDRH3 regions using principal component analysis (PCA) of Kidera factors18, which are a set of independent factors encapsulating information from 188 different biophysical characteristics of the 20 amino acids. We observed clear differences in the CDRH3 protein structure between GC B cells and PCs as well as between IgG1-switched and IgE-switched clones in wild-type mice (Fig. 6d), indicating that the majority of IgE^+ PC clones were of extra-follicular origin and had switched directly from IgM to IgE. This was supported by clonal analysis, which indicated that <30% of IgE^+ PC clones were shared with $IgG1^+$ PC clones and only around 30% of IgE^+ PC clones were shared with IgE^+ GC clones (Supplementary Fig. 6b,c). Furthermore, Kidera PCA showed that the properties of IgE and IgG1 in *Tcrd*$^{-/-}$ mice were different from

those of wild-type mice, suggesting that immune-surveillance by γδ T cells had a role in selecting the physiochemical properties of the CDRH3 regions (Fig. 6d).

Selection events are also expected to shape the B cell repertoire in terms of V, D, J gene-usage. We found that only 5 major IgHV and 5 IgHD family genes were commonly used, but all 4 IGHJ genes were used for both $IgG1^+$ and IgE^+ GC B cells and PCs (Supplementary Fig. 6d-f). The third most frequent D gene in both IgE^+ and $IgG1^+$ GC B cells and PCs could not be annotated by IMGT, most likely due to an IGHD gene in the FVB genome that is absent from the IMGT genomic data, as the heavy chain repertoire is highly variable between inbred strains19. We annotated this new gene as Dx. 3D analysis of VDJ usage in IgE^+ PCs indicated that V1D2 was the dominant selection (Fig. 6e), consistent with data showing that the IgHV1 family is most frequently used in mouse Ig19, 20. J usage was approximately equal between the 4 J family groups (Fig. 6e). The VDJ analysis also revealed that some VDJ combinations in wild-type mice, particularly the novel V3Dx segment, were significantly less selected in IgE^+ PCs from *Tcrd*$^{-/-}$ mice (Fig. 6e-g).

We next compared the physicochemical properties of CDRH3 in the wild-type V3Dx clones with those of V3D2 clones, which used the same V but different D gene, V1D2 clones, which were the most common selection and V14D2 clones, which did not require γδ T cell selection. Kidera factor PCA indicated that the V3Dx clones had unique CDRH3 physicochemical characteristics (Fig. 6h) and contained a lower frequency of aromatic and small amino acids, but a higher frequency of aliphatic and basic amino acids, as well as a higher isoelectric point than clones of the other VD combinations (Fig. 6i). These characteristics suggest that the antigen-binding site was hydrophobic, with slight positive charge in the loop at blood pH. In addition, the V3Dx-expressing clones had shorter CDRH3 regions than the V1D2 and V3D2 clones (Fig. 6i), indicating antigen selection21, 22, and carried fewer mutations (Fig. 6j), indicating they were more germline in nature. In sum, this data indicates that in response to DMBA, $γδTCR^+$ T cells shaped the IgE repertoire by supporting specific VDJ rearrangements, resulting in unique characteristics of the CDRH3 antigen-binding site that suggests polyreactive autologous binding.

DMBA-induced IgE is autoantigenic and differs from TPA-induced IgE

We next explored whether the IgE responses induced by topical DMBA were auto-reactive. We screened the binding of IgE, from serum of DMBA-treated wild-type mice, to human HEp2 cells and observed several strong staining patterns (Fig. 7a and Supplementary Fig. 7a), indicating both autoreactivity and cross-species reactivity of IgE. The most common staining patterns of IgE on HEp2 cells were ‘nuclear dots’, which indicate anti-nuclear specificity and ‘cytoplasmic vesicles’ that resembled stress granules (Fig. 7a and Supplementary Fig. 7a). In addition, we detected IgE reactivity towards ds-DNA (Fig. 7b) and towards damaged epithelial cells, frequently around hair-follicles, in epidermal sheets from *FceR1a*$^{-/-}$ mice isolated 24hr after DMBA exposure (Supplementary Fig. 7f-g). We detected no autoreactivity against HEp2 cells with IgE from serum of DMBA-treated *Tcrd*$^{-/-}$ mice or IgE from serum of wild-type mice treated topically with 12-*O*-tetradecanoylphorbol-13-acetate (TPA) (Fig. 7a and Supplementary Fig. 7b,c), which did not provoke epithelial cell DNA-damage (Fig. 7c), but triggers general skin inflammation.

We next sorted $FSC^{hi}CD95^{hi}CD138^{+}$ PCs from the skin draining LNs of wild-type mice exposed topically to DMBA or TPA and compared their IgE heavy-chain repertoires using high-throughput sequencing. Alakazam analysis indicated that TPA-induced IgE^{+} PCs exhibited significantly less diversity throughout the repertoire compared to DMBA-induced IgE^{+} PCs (Fig. 7d). Kidera factor PCA indicated more heterogeneity in the CDRH3 regions of TPA-induced IgE compared with DMBA-induced IgE, with little overlap between the two responses (Fig. 7e). In parallel, VDJ gene family-usage amongst TPA-induced IgE was dominated by V1 genes, with significantly less selection for V3 and V14 genes compared to DMBA-induced IgE (Fig. 7f,g). Notably, TPA also did not generate the V3Dx-expressing clones, which we had found to be promoted by γδ T cells in response to DMBA-induced DNA-damage (Fig. 7g). Together these results indicate, that skin exposure to DMBA drove a unique, autoreactive IgE repertoire that was distinct from that induced in response to TPA, which induced local acute inflammation.

Discussion

Here we found that IgE was rapidly induced by cutaneous exposure to the carcinogen DMBA and accumulated in the skin and tumors on FcεRI-expressing basophils. The IgE response required $\gamma\delta TCR^{+}$ IELs, was autoreactive and protective against epithelial carcinogenesis. FcεRI-expressing cells also accumulated in human skin SCCs and expression level correlated with disease severity. Together, our data indicate that IgE contributes to early tissue immune-surveillance against environmental xenobiotics or toxins and has a protective role against epithelial tumor development.

Polyaromatic hydrocarbons such as DMBA are ubiquitous and arise from many sources, including car emissions and tobacco smoke14, 15. They are the main organic constituent in air pollution, and their levels correlate with the prevalence and severity of atopic dermatitis23, 24. In mice, chronic skin exposure to air pollutants can induce atopic dermatitis-like features and IgE production. However, whilst the skin gene expression depends on ligation of the aromatic hydrocarbon receptor (AhR) by polyaromatic hydrocarbons, the increase in IgE does not25. Consistent with this, we found that initiation of IgE after topical DMBA depended on epithelial DNA-damage and not direct AhR engagement. Host DNA can selectively induce IgE26, suggesting that dying cells have unique IgE adjuvant activity. Furthermore, expression of autologous stress-antigens, such as NKG2D-ligands, on damaged skin epithelia promotes IgE production12. Topical TPA also induces NKG2D-ligand expression27, which may partly explain the induction of IgE by this agent. However, sequencing analysis revealed that different types of tissue-damage initiate distinct IgE repertoires. In humans, self-reactive IgE have been found in patients with systemic lupus erythematous28, 29, bullous pemphigoid30, atopic dermatitis31 and primary immune deficiencies32. These data suggests that IgE responses are potently promoted by autologous cell stress and/or damage, which is induced by skin exposure to environmental xenobiotics.

IELs provide a ‘first line of defense’ in epithelial tissues. A large proportion of IELs carry γδTCRs and are autoreactive in nature as they express receptors for tissue-specific stress-molecules33. We show that following DMBA-induced epithelial damage IELs elicited rapid

IgE in the parafollicular regions and subsequently triggered a conventional adaptive response requiring polyclonal αβTCR$^+$ CD4$^+$ T cells producing IL-4. This mode of IgE induction differs from regulation of self-reactive 'natural IgE', which is also γδ T cell-driven, but is independent of αβ T cells and MHCII34, 35. Deep-sequencing of IgG1$^+$ and IgE$^+$ GC B cells and PCs demonstrated that γδ T cells shaped the repertoire and the nature of the antibodies produced. Thus, antibody deep-sequencing revealed a previously unrecognized mode of B cell selection dictated by tissue-resident IELs.

γδ T cells and tissue-specific γδIELs are key players in host defense against cancer, which is considered to reflect innate properties such as cytotoxicity and cytokine production11, 13, 27. Here we show that they can provide a 'second line of host defense' via initiation of adaptive autoreactive IgE responses and FcεRI-expressing effector cells. Our findings that endogenous IgE can suppress tumor growth are supported by evidence that immunization with tumor antigen-specific IgE can eradicate tumors and is more effective than IgG136, 37. How IgE inhibits tumor growth in our model remains to be determined, however it required FcεRI expression and mast cells were not essential, suggesting it may involve soluble factors and/or cytotoxicity mediated by basophils.

In humans, epithelial skin cancers are on the rise38, 39. In addition to UV-irradiation, environmental chemical carcinogens can also lead to skin SCC development, as indicated by the causal link between scrotal SCC and soot exposure, which contains polyaromatic hydrocarbons, in chimney sweeps40. Moreover, tobacco smokers, who are exposed to high amounts of polyaromatic benz[a]antracene, have a 50% increased likelihood of developing skin SCC41. Studies on IgE and cancer risk in humans show a significant, albeit weak, negative correlation between serum IgE and overall cancer risk42, 43. In addition, *FceR1a* was reported among the top 50 genes associated with positive survival in 39 human malignancies44. The presence of intratumoral γδ T cells was the most favorable prognostic indicator of cancer survival44, while a high number of infiltrating PCs was also strongly associated with good clinical outcome44. Consistent with these observations, we found that FcεRI-expressing cells were abundant in human SCCs and there was an inverse correlation between expression of *FceR1a* and more advanced disease. Of note, the use of omalizumab, a mAb blocking IgE, has been associated with more frequent development of cancer, particularly epithelial and solid organ cancers45.

Together these findings suggest that the IgE-FcεRI axis is part of a tumor-protective immune response and provides support for the 'toxin hypothesis', which proposes that IgE is a host defense mechanism against non-infectious cell-damaging environmental xenobiotics.

Methods

Mice

Genetically altered mice were generated as previously described. *Tcrd*$^{-/-}$46, *Tcrb*$^{-/-}$47, *Il4*$^{-/-}$48, Langerin-DTA49 (LC-deficient) and *Vg5Vd1*$^{-/-}$50,51 were on the FVB/N background after > 10 backcrosses; *Igh-7*$^{-/-}$52, *FceR1a*$^{-/-}$53 and *Cpa3*$^{Cre/+}$54 were on the BALB/c background after >10 backcrosses; and OTII Tg55, *Tcrb*$^{-/-}$56, CD19-Cre57 and Bcl6$^{fl/fl}$58 were on the C57BL/6 background. Strain-matched wild-type control animals

were purchased from Charles River. Mice were bred and maintained in individually ventilated cages under specific pathogen-free conditions. Age-matched, female mice were used for all experiments at ≥ 7 weeks of age and selected at random from a large pool when allocated to experiments. All studies were approved by Imperial College AWERB (Animal Welfare and Ethical Review Body) and by the UK Home Office. Experiments involving cancer studies strictly adhered to the guidelines set out by the National Cancer Research Institute (NCRI) and Workman et al. in 'Guidelines for the Welfare and Use of Animals in Cancer Research'59. All studies using animals were conducted following the Animal Research: Reporting In Vivo Experiments (ARRIVE) guidelines60.

Chemical cutaneous damage and carcinogenesis

Chemicals 7,12-Dimethylbenz[a]anthracene (DMBA) and 12-0-tetradecanoylphorbol-13-acetate (TPA) were purchased from Sigma and dissolved in acetone and 100% ethanol respectively. Acute damage was induced by exposing the dorsal sides of the ear skin to a single or repeated 200nM dose of DMBA or 2.5nM dose of TPA, in 25μl.

For cutaneous carcinogenesis age-matched female mice were used at 7 weeks of age. The dorsal back area was shaved with a surgical blade and mice rested for 1 week. Applications of chemicals and tumor monitoring were performed as previously described13. In brief, 200nM DMBA was carefully and slowly applied by pipette, in a 100 μl volume, to the entire shaved skin area. Mice were rested for one week and 100nM DMBA then applied weekly. Hair regrowth during the experiment was gently removed by clipping with trimmers. Mice were monitored daily and cutaneous tumors were counted and measured with a caliper once weekly. Back skin and tumors were evaluated by visual inspection by an observer blinded to the experimental groups.

UV-irradiation

The back skin of FVB mice was shaved using electrical clippers 3 days before UV-irradiation. Mice were exposed to the UV light source in their cages placed under four 100 W UV lamps with the spectral output 270-350 nm (predominantly UVB) (Philips TL12 lamps). The total dose of UVB radiation was monitored during each exposure using an IL-400 A UVB photometer (International Light). Mice were given 100mJ/cm^2 three times a week.

Tissue Processing

Tissue was cut into small 1mm^2 pieces using a scalpel blade and incubated for 2 hrs in digestion buffer containing 25ug/ml Liberase (Roche), 250ug/ml DNAseI (Roche) and 1x DNAse buffer (1.21 Tris base, 0.5g $MgCl_2$ and 0.073g $CaCl_2$) at 37°. Following digestion, tissue was transferred into C-tubes (Miltenyi Biotech) containing RPMI-1640 media (Thermo Fisher) supplemented with 10% heat-inactivated foetal calf serum, 1% Penicillin-Streptomycin-Glutamine (Thermo Fisher) and physically disrupted using a Miltenyi cell dissociator. Cell suspensions were then filtered and cells counted using a CASY cell counter (Roche).

Europe PMC Funders Author Manuscripts

Flow cytometry

Cell suspensions were blocked for non-specific binding using antibody against FcγR (2.4G2) and 2% normal rat serum (Sigma) prior to any staining protocols. For staining of cell surface markers, cell suspensions were stained with fluorochrome-conjugated antibodies or appropriate isotype control with the addition of a fixable, live/dead discrimination dye (Invitrogen) for 25 min and subsequently washed. Intracellular staining was then carried out using an Intracellular Staining kit as per manufacturer's instruction (ThermoFisher Scientific). Cells were fixed for 10 min at 4°C, washed with Perm buffer and stained for intracellular markers for 25 min. For intranuclear γH2AX staining, cells were fixed/permeablized in ice-cold 70% ethanol at -20°C for 2 hrs, blocked with 2% normal mouse serum (Sigma), Fc-block and 2% fetal calf serum for 15 min, followed by 45 min staining for γH2AX at room temperature. Stained cells were analyzed using BD FACSVerse and Fortessa X20 (BD Biosciences, NJ, USA) machines. Data analysis was performed using FlowJo 10 for Mac (TreeStar, OR, USA).

Antibodies were sourced from eBioscience unless otherwise stated. The following antibodies were used: anti-CD45 (30-F11), anti-B220 (RA3-6B2), anti-CD38 (90/CD38, BD), anti-CD138 (281-2, BD), anti-CD95 (Jo2), anti-GL7 (GL-7), anti-CD3 (145-2C11, Biolegend), anti-IgE (23G3), anti-IgG1 (M1-14D12), anti-IgG2a (R19-15, BD), anti-TCRβ (H57-597), anti-TCRγδ (eBioGL3), anti-Vγ5 (536), anti-Vγ4 (UC3-10Ab, Biolegend), anti-CD117 (2B8), anti-CD41 (MWReg30, Biolegend), anti-FcεRI (MAR-1, Biolegend), anti-IL-4 (11B11), anti-IL-6 (MP5-20F3, Biolegend), anti-CD63 (NVG-2, Biolegend) and γH2AX (JBW301, Millipore).

ELISA

For IgG1 and IgG2a antibodies, NUNC Immune Maxisorp 96-well plates (Thermo Scientific) were coated with 5 μg/ml goat anti-mouse IgH+L (Southern Biotech) in borate buffered saline at 37°C for 3hr. After washing, plates were blocked with PBS containing 0.5% BSA for 1 hr at room temperature, and appropriately diluted sera added and incubated overnight at 4°C. After washing, plates were incubated with alkaline phosphatase-conjugated polyclonal goat anti-mouse IgG1 or IgG2a (also detects IgG2c in C57BL/6 mice) (both Southern Biotech) for 5 hr at 4°C. Following further washing, the alkaline phosphatase substrate pNPP (Sigma) was added and absorbance measured at 405 nm. Total IgE was measured by an IgE capture method. Sera to be tested and IgE standard were added to plate wells coated with 1 μg/ml rat monoclonal anti-mouse IgE (PharMingen) and blocked with 1% rat serum. Biotinylated rat monoclonal anti-mouse IgE (PharMingen) at 1 μg/ml were then added and incubated for 2h at 37°C. After washing in PBS 0.05% Tween, plates were incubated with alkaline phosphatase-conjugated Streptavidin (PharMingen) for 1 hr at 37°C. After washing, detection of antibody levels was carried out by addition of alkaline phosphatase substrate pNPP (Sigma) and absorbance measured at 405 nm.

For IgE ds-DNA autoreactivity, MaxiSorp plates were coated with 1 μg/ml rat monoclonal anti-mouse IgE (PharMingen) and blocked with 1% rat serum and 3% milk. Serum samples were screened at 1:25 dilution. 100 ng/ml biotinylated herring sperm ds-DNA (Promega) was then added and incubated overnight at 4°C. After washing in PBS 0.05% Tween, plates

were incubated with alkaline phosphatase-conjugated Streptavidin (PharMingen) for 1 hr at 37°C. After washing, detection was carried out by addition of alkaline phosphatase substrate pNPP (Sigma) and absorbance measured at 405 nm. Autoantibody levels were expressed in arbitrary ELISA units.

HEp-2 staining

Auto-reactivity of IgE was tested by indirect immunofluorescence using HEp-2 cells. Serum samples were diluted appropriately (tested in dilutions between neat – 1:25, depending on IgE titers) and incubated on HEp-2 slides (Bio-Rad) overnight at 4°C. After washing in PBS, slides were incubated with purified rat anti-mouse IgE (BD) for 2hrs, washed again and further incubated with anti-rat 555 secondary antibody (ThermoFisher) for 1hr at room temperature. As controls, serum from similarly treated IgE-deficient mice was also assessed as well as naïve wild-type serum. Slides were thoroughly washed and mounted with Vectashield containing DAPI (Vectashield) and visualised with a Leica DM4 fluorescence microscope (Leica).

Immunofluorescent staining of tumor samples

Tumors were removed from the back along with a small piece of adjacent skin and snap frozen in OCT on dry ice. 6 μm sections were cut using a Leica JUNG CM1800 cryostat and stored at -80ºC. For staining, slides were returned to room temperature before fixation with 4% paraformaldhyde for 15min. Samples were then blocked in 5% goat serum for 1 hr at room temperature before staining with rat anti-mouse IgE (BD) overnight at 4°C. Following staining, samples were washed and incubated with alexa-fluor 555 conjugated, goat anti-rat IgE (ThermoFisher). After extensive washing, samples were mounted in VectaShield containing DAPI (Vectashield) and visualised with a Leica SP5 confocal laser-scanning microscope (Leica).

Epidermal sheets

Ears were collected, split into dorsal and ventral sides and floated dermis side-down in 0.5 M NH_4SCN for 40 minutes, 37°C, 5% v/v CO_2. Subsequently, intact epidermal sheets were isolated and washed in PBS. They were then fixed in ice-cold acetone at -20°C for 15 minutes, followed by rehydration in PBS. Non-specific binding to the epidermal tissue was blocked with 2% BSA for 1 hr and then 1:25 dilution of test sera was added and incubated overnight at 4°C. Any IgE binding to the tissue was visualized by first incubating with rat anti-mouse IgE (BD) followed by alexa-fluor 555 conjugated, goat anti-rat IgE both for 1 hr at room temperature. After extensive washing in PBS, samples were mounted in VectaShield containing DAPI (Vectashield) and visualised with a Leica SP5 confocal laser-scanning microscope (Leica).

Adoptive Transfer experiments

Whole $CD4^+$ T cells were isolated from the spleens of donor wild-type and *Il4*$^{-/-}$ mice (using Miltenyi MACS isolation kits). For OTII transfer experiments, OTII Tg $CD4^+$ T cells were cell sorted using OVA-peptide loaded tetramers (NIH, tetramer facility). $2x10^6$ cells were

intravenously injected, mice were rested for 24 hr and the dorsal ear skin then exposed to DMBA as described above.

BM chimeras

Wild-type, *Tcrd*$^{+/-}$ and *Il4*$^{-/-}$ mice were sub-lethally irradiated (750 rad) and immediately reconstituted with 5x10^{6} donor BM cells by intravenous injection. Mice were left for 8 weeks to fully reconstitute the haematopoietic cells, and then exposed to DMBA on the skin as described. Chimerism was assessed by FACS analysis of peripheral lymph nodes and skin tissue at the end of the experiments.

qRT-PCR and primer sequences

RNA was extracted from ammonium-fixed epidermis, or tumor tissue, preserved in RNA-later, using an RNEasy Mini kit (Qiagen). RNA was dissolved in nuclease-free water, and yield and purity were determined. Complementary DNA (cDNA) was synthesised from RNA with an iScript cDNA synthesis kit (Bio-Rad) as per the manufacturer's instructions. cDNA was diluted in nuclease-free double-deionized water for qRT–PCR. All primers were single-stranded DNA oligonucleotides (Sigma) that were intron-spanning as verified by NCBI Primer-Blast tool. Real-time PCR product was detected with SYBR Green (Life) measured continuously with a ViiA 7 Real-Time PCR system (Applied Biosystems, CA, USA). Ct values for genes of interest were normalized against Ct values of the housekeeping gene Cyclophilin (Cyc) using the $2^{-\Delta Ct}$ method. The following primers were used: IgE: F (5'-CAAGTCAGCCAAGAACTTCAC-3'), R (5'-GACAGGTCGAACTAGGATAGTC-3'), IgG1: F (5'-TTGCATATGTACAGTCCCAG-3'), R (5'-GTCAGAGTAATGGTGAGCAC-3'), IgM: F (5'-AAGACTGGAATAACAGGAAGGA-3'), R (5'-GTTTGTGCACCTCATTGGG-3'), Rae1: F (5'-TGGACACTCACAAGACCAATG-3'), R (5'-CCCAGGTGGCACTAGGAGT-3'), IL-4: F (5'-CATCGGCATTTTGAACGAG-3'), R (5'-CGAGCTCACTCTCTGTGGTG-3'), IL-6: F (5'-TGATGGATGCTACCAAACTGG-3'), R (5'-TTCATGTACTCCAGGTAGCTATGG-3'), IL-33: F (5'-CACATTGAGCATCCAAGGAA-3'), R (5'-AACAGATTGGTCATTGTATGTACTCAG-3'), Cyc: F (5'-CAAATGCTGGACCAAACACAA-3'), R (5'-CCATCCAGCCATTCAGTCTTG-3').

Immunoglobulin sequencing and analysis

Mice were treated twice with DMBA or TPA to the dorsal side of the ear skin, 3 days apart. One week after the last exposure, draining-LNs were collected and germinal center B cells ($B220^{+}CD95^{+}GL7^{+}$) and plasma cells ($FSC^{hi}CD95^{hi}CD138^{+}$) cell sorted on a BD FACS Aria III (BD Biosciences, NJ, USA). RNA was extracted using RNEasy Micro kits (Qiagen) and reverse transcriped using SuperScript™ III Reverse Transcriptase (ThermoFisher). Sequences were amplified using Phusion High-Fidelity DNA Polymerase (NewEngland Biolabs) to ensure accuracy and robust performance for large PCR products. PCR with a primer in the constant Cε region 5'-CTAGGGTCATGGAAGCAGTGCC-3' or Cγ1 region 5'-GGGAAATAGCCCTTGACCAGG-3' in combination with a promiscuous V region primer (binding all Vh genes) 5'-GAGGTGCAGCTGCAGGAGTCTGG-3' was performed. All primers were labeled at either end with Multiplex Identifiers (MIDs) for multiplexing. PCR thermal cycling was as follows: 98°C, 30 sec; 30x (98°C, 30 sec; 60°C, 30 sec; 72°C,

35 sec); and 72°C, 10min. Amplicons were purified by gel extraction using QIAquick PCR purification kit (Qiagen) and deep-sequenced by long-read 454 pyrosequencing on the Genome Sequencer FLX system (Roche). Raw sequencing data was presented in .FASTA format and unproductive sequences removed (data cleanup stages as described61).

Analysis was performed as previously described61. In short: sequences were assigned to individual samples according to their MID. V(D)J gene assignment of individual sequences were annotated using IMGT/HighV-Quest and the mouse database. Mean values of V(D)J gene usage were calculated before 3D bubble plots were created using the R package *plot3D*. Repertoire diversity was characterized using the Hill diversity index62, 63 and plotted using the Alakazam package17. Physiochemical properties of the CDRH3 region were calculated using the R package Peptides. Physiochemical properties included length, isoelectric point (pI), frequencies of amino acid classes in the CDRH3 region, and Kidera factors. Kidera factors are a set of 10 independent factors encapsulating information from ~180 different measurable biophysical characteristics of the 20 amino acids18. Principal component analysis of Kidera factors was performed using the *prcomp* function in R using Minkowski distances as previously described64.

Human tissue

For FACS analysis, freshly excised SCC tissue and peripheral blood were obtained from 12 patients during surgery at the Dermatology Department, University Hospital Southampton NHS Foundation Trust. Ethics were provided by the South Central Hampshire B NRES Committee (reference number 07/H0504/187). All participants recruited to the study provided informed consent for blood and tissue samples to be used for research purposes. All tumor tissue used in the study was confirmed SSCs with a diameter > 8mm. Non-lesional skin was histopathologically normal and > 6mm away from the tumor edge. To obtain single cell suspension, tumor samples were cut into small pieces and enzymatically digested with 1 mg/ml collagenase I-A (Sigma) and 10 μg/ml DNAse I (Sigma) in RPMI medium at 37°C for 1.5 hours. The resulting suspension was passed through 70μm cell strainers and centrifuged in Optiprep (Axis-Shield). PBMCs were isolated from venous blood from the SCC patients by centrifugation with Lymphoprep (Axis-Shield). Single cell suspensions were stained for FACS against CD45 (2D1) and FcεR1 (MHE-18) (both BioLegend). Cells were gated on FSC and SSC and dead cells excluded using near IR live/dead stain (Invitrogen).

For immunohistochemistry on human SSC tissue; 5μm tissue sections were cut from formalin-fixed paraffin-embedded samples and placed onto 3-aminopropyltriethoxysilane (APES)-coated microscope slides. Sections were deparaffinised in xylene and rehydrated through graded alcohols. Endogenous peroxidase was inhibited with 0.5% hydrogen peroxide, prior to antigen retrieval by microwaving in 10 mM citrate buffer, pH 6. Endogenous avidin and biotin were blocked (Vector Labs), before Dulbecco's Modified Eagle's Medium (Gibco) containing 1% bovine serum albumin (Sigma) and 20% foetal bovine serum (Gibco) blocking medium was applied. Primary antibody (FcER1 (9E1), 1:20 dilution (Abcam)) was then left on the sections for 16 hours at 4°C before 3 Tris buffered saline (TBS) washes, followed by application of biotinylated goat anti-mouse (1:400

dilution, Jackson ImmunoResearch) for 30 minutes. After 3 TBS washes, streptavidin-biotin complexes (Vector Labs) were applied, before being washed with TBS x 3 and application of diaminobenzidine (DAKO). After washing with TBS, sections were counterstained with Mayer's Haematoxylin (Sigma) and dehydrated through graded alcohols and xylene. Sections were mounted in DPX mountant (Sigma) and coverslips applied. Slides were imaged at 2x and 20x magnification using an Olympus Dotslide microscope and analysed using OlyVIA software.

For SSC tumor gene expression, fixed frozen paraffin embedded skin samples from 56 patients obtained from the University of Dundee, Tayside NHS Trust and Greater Glasgow and Clyde NHS Trust were analyzed. The study was conducted according to the Declaration of Helsinki Principles and all patients donating samples to this study provided written, informed consent in accordance with ethical approval from the East of Scotland Research Ethics Service (EoSRES) REC 1. SSC tumors were graded by an experienced dermatopathologist as low risk or high risk based on the Scottish Intercollegiate Guidelines Network for cutaneous SCC. In addition, peri-lesional skin (histopathologically normal looking skin > 4 mm away from the tumor edge) and abdominal non-UV exposed skin were also analyzed. Total RNA was extracted using Qiagen RNeasy extraction kit and directly hybridized using the NanoString PanCancer and PanCancer Immune expression panel and analyzed on a nCounter (NanoString).

Statistical evaluation

The statistical significance of difference between experimental groups was determined using two-tailed Student's t-test for unpaired data, Wilcoxon test for paired samples, one-way ANOVA or linear regression, where appropriate, with results deemed significant at $p<0.05$. Stars of significance correlate to: *$p<0.05$; **$P<0.01$; ***$P<0.001$ and ****$p<0.0001$. Statistics was performed with GraphPad Prism 6.00 for Mac (GraphPad; La Jolla, CA, USA).

Supplementary Material

Refer to Web version on PubMed Central for supplementary material.

Acknowledgements

We thank B. Norzawani, C. Margreitter, C. Townsend and B. Hunt for computational assistance and advice during antibody sequencing analysis, and H.R. Rodewald and A. Hayday for providing *Cpa3*$^{Cre/+}$ and *Vg5Vd1*$^{-/-}$ mice respectively. We are indebted to the staff of the Imperial Central Biomedical Services for the care of the animals and the LMS/NIHR Imperial Biomedical Research Centre Flow Cytometry Facility for FACS support. We are grateful to A. Mowat for critical reading of the manuscript and the informed advice of many close colleagues. This work was supported by the Wellcome Trust (100999/Z/13/Z) and in part by the Cancer Research UK (C21010/A19788) and the NIHR Newcastle Biomedical Research Centre. Chester Lai was supported by a Wellcome Trust Research Training Fellowship.

References

1. Vernersson M, Aveskogh M, Hellman L. Cloning of IgE from the echidna (Tachyglossus aculeatus) and a comparative analysis of epsilon chains from all three extant mammalian lineages. Dev Comp Immunol. 2004; 28:61–75. [PubMed: 12962983]

Europe PMC Funders Author Manuscripts

2. Harris N, Gause WC. To B or not to B: B cells and the Th2-type immune response to helminths. Trends in immunology. 2011; 32:80–88. [PubMed: 21159556]
3. Profet M. The function of allergy: immunological defense against toxins. The Quarterly review of biology. 1991; 66:23–62. [PubMed: 2052671]
4. Marichal T, et al. A beneficial role for immunoglobulin E in host defense against honeybee venom. Immunity. 2013; 39:963–975. [PubMed: 24210352]
5. Palm NW, et al. Bee venom phospholipase A2 induces a primary type 2 response that is dependent on the receptor ST2 and confers protective immunity. Immunity. 2013; 39:976–985. [PubMed: 24210353]
6. Starkl P, et al. IgE antibodies, FcepsilonRIalpha, and IgE-mediated local anaphylaxis can limit snake venom toxicity. J Allergy Clin Immunol. 2016; 137:246–257 e211. [PubMed: 26410782]
7. Palm NW, Rosenstein RK, Medzhitov R. Allergic host defences. Nature. 2012; 484:465–472. [PubMed: 22538607]
8. Dalessandri T, Strid J. Beneficial autoimmunity at body surfaces - immune surveillance and rapid type 2 immunity regulate tissue homeostasis and cancer. Frontiers in immunology. 2014; 5:347. [PubMed: 25101088]
9. Strid J, Hourihane J, Kimber I, Callard R, Strobel S. Disruption of the stratum corneum allows potent epicutaneous immunization with protein antigens resulting in a dominant systemic Th2 response. European journal of immunology. 2004; 34:2100–2109. [PubMed: 15259007]
10. Nelde A, et al. The impact of the route and frequency of antigen exposure on the IgE response in allergy. Int Arch Allergy Immunol. 2001; 124:461–469. [PubMed: 11340329]
11. Dalessandri T, Crawford G, Hayes M, Castro Seoane R, Strid J. IL-13 from intraepithelial lymphocytes regulates tissue homeostasis and protects against carcinogenesis in the skin. Nat Commun. 2016; 7:12080. [PubMed: 27357235]
12. Strid J, Sobolev O, Zafirova B, Polic B, Hayday A. The intraepithelial T cell response to NKG2D-ligands links lymphoid stress surveillance to atopy. Science. 2011; 334:1293–1297. [PubMed: 22144628]
13. Strid J, et al. Acute upregulation of an NKG2D ligand promotes rapid reorganization of a local immune compartment with pleiotropic effects on carcinogenesis. Nature immunology. 2008; 9:146–154. [PubMed: 18176566]
14. Kim KH, Jahan SA, Kabir E, Brown RJ. A review of airborne polycyclic aromatic hydrocarbons (PAHs) and their human health effects. Environ Int. 2013; 60:71–80. [PubMed: 24013021]
15. Totlandsdal AI, et al. Differential effects of the particle core and organic extract of diesel exhaust particles. Toxicol Lett. 2012; 208:262–268. [PubMed: 22100492]
16. Modi BG, et al. Langerhans cells facilitate epithelial DNA damage and squamous cell carcinoma. Science. 2012; 335:104–108. [PubMed: 22223807]
17. Gupta NT, et al. Change-O: a toolkit for analyzing large-scale B cell immunoglobulin repertoire sequencing data. Bioinformatics. 2015; 31:3356–3358. [PubMed: 26069265]
18. Nakai K, Kidera A, Kanehisa M. Cluster analysis of amino acid indices for prediction of protein structure and function. Protein Eng. 1988; 2:93–100. [PubMed: 3244698]
19. Collins AM, Wang Y, Roskin KM, Marquis CP, Jackson KJ. The mouse antibody heavy chain repertoire is germline-focused and highly variable between inbred strains. Philos Trans R Soc Lond B Biol Sci. 2015; 370
20. Rogosch T, et al. Plasma cells and nonplasma B cells express differing IgE repertoires in allergic sensitization. J Immunol. 2010; 184:4947–4954. [PubMed: 20363970]
21. Rosner K, et al. Third complementarity-determining region of mutated VH immunoglobulin genes contains shorter V, D, J, P, and N components than non-mutated genes. Immunology. 2001; 103:179–187. [PubMed: 11412305]
22. Luger E, et al. Somatic diversity of the immunoglobulin repertoire is controlled in an isotype-specific manner. European journal of immunology. 2001; 31:2319–2330. [PubMed: 11477544]
23. Kim J, et al. Symptoms of atopic dermatitis are influenced by outdoor air pollution. J Allergy Clin Immunol. 2013; 132:495–498 e491. [PubMed: 23763977]

24. Morgenstern V, et al. Atopic diseases, allergic sensitization, and exposure to traffic-related air pollution in children. Am J Respir Crit Care Med. 2008; 177:1331–1337. [PubMed: 18337595]
25. Hidaka T, et al. The aryl hydrocarbon receptor AhR links atopic dermatitis and air pollution via induction of the neurotrophic factor artemin. Nature immunology. 2017; 18:64–73. [PubMed: 27869817]
26. Marichal T, et al. DNA released from dying host cells mediates aluminum adjuvant activity. Nat Med. 2011; 17:996–1002. [PubMed: 21765404]
27. Girardi M, et al. Regulation of cutaneous malignancy by gammadelta T cells. Science. 2001; 294:605–609. [PubMed: 11567106]
28. Dema B, et al. Immunoglobulin E plays an immunoregulatory role in lupus. The Journal of experimental medicine. 2014; 211:2159–2168. [PubMed: 25267791]
29. Henault J, et al. Self-reactive IgE exacerbates interferon responses associated with autoimmunity. Nature immunology. 2016; 17:196–203. [PubMed: 26692173]
30. Messingham KA, Holahan HM, Fairley JA. Unraveling the significance of IgE autoantibodies in organ-specific autoimmunity: lessons learned from bullous pemphigoid. Immunol Res. 2014; 59:273–278. [PubMed: 24845463]
31. Altrichter S, et al. Serum IgE autoantibodies target keratinocytes in patients with atopic dermatitis. The Journal of investigative dermatology. 2008; 128:2232–2239. [PubMed: 18480840]
32. Ozcan E, Notarangelo LD, Geha RS. Primary immune deficiencies with aberrant IgE production. J Allergy Clin Immunol. 2008; 122:1054–1062. quiz 1063-1054. [PubMed: 19084106]
33. Vantourout P, Hayday A. Six-of-the-best: unique contributions of gammadelta T cells to immunology. Nat Rev Immunol. 2013; 13:88–100. [PubMed: 23348415]
34. Wen L, et al. Germinal center formation, immunoglobulin class switching, and autoantibody production driven by "non alpha/beta" T cells. The Journal of experimental medicine. 1996; 183:2271–2282. [PubMed: 8642336]
35. McCoy KD, et al. Natural IgE production in the absence of MHC Class II cognate help. Immunity. 2006; 24:329–339. [PubMed: 16546101]
36. Josephs DH, et al. Anti-Folate Receptor-alpha IgE but not IgG Recruits Macrophages to Attack Tumors via TNFalpha/MCP-1 Signaling. Cancer research. 2017; 77:1127–1141. [PubMed: 28096174]
37. Josephs DH, Spicer JF, Karagiannis P, Gould HJ, Karagiannis SN. IgE immunotherapy: a novel concept with promise for the treatment of cancer. MAbs. 2014; 6:54–72. [PubMed: 24423620]
38. Rogers HW, et al. Incidence estimate of nonmelanoma skin cancer in the United States, 2006. Archives of dermatology. 2010; 146:283–287. [PubMed: 20231499]
39. Goon PK, Greenberg DC, Igali L, Levell NJ. Squamous Cell Carcinoma of the Skin has More Than Doubled Over the Last Decade in the UK. Acta Derm Venereol. 2016; 96:820–821. [PubMed: 26631391]
40. Lippman SM, Hawk ET. Cancer prevention: from 1727 to milestones of the past 100 years. Cancer research. 2009; 69:5269–5284. [PubMed: 19491253]
41. Leonardi-Bee J, Ellison T, Bath-Hextall F. Smoking and the risk of nonmelanoma skin cancer: systematic review and meta-analysis. Archives of dermatology. 2012; 148:939–946. [PubMed: 22711192]
42. Van Hemelrijck M, et al. Immunoglobulin E and cancer: a meta-analysis and a large Swedish cohort study. Cancer Causes Control. 2010; 21:1657–1667. [PubMed: 20533084]
43. Sherman PW, Holland E, Sherman JS. Allergies: their role in cancer prevention. The Quarterly review of biology. 2008; 83:339–362. [PubMed: 19143335]
44. Gentles AJ, et al. The prognostic landscape of genes and infiltrating immune cells across human cancers. Nat Med. 2015; 21:938–945. [PubMed: 26193342]
45. Strunk RC, Bloomberg GR. Omalizumab for asthma. N Engl J Med. 2006; 354:2689–2695. [PubMed: 16790701]
46. Itohara S, et al. T cell receptor delta gene mutant mice: independent generation of alpha beta T cells and programmed rearrangements of gamma delta TCR genes. Cell. 1993; 72:337–348. [PubMed: 8381716]

47. Mombaerts P, Clarke AR, Hooper ML, Tonegawa S. Creation of a large genomic deletion at the T-cell antigen receptor beta-subunit locus in mouse embryonic stem cells by gene targeting. Proc Natl Acad Sci U S A. 1991; 88:3084–3087. [PubMed: 1826563]
48. Kuhn R, Rajewsky K, Muller W. Generation and analysis of interleukin-4 deficient mice. Science. 1991; 254:707–710. [PubMed: 1948049]
49. Kaplan DH, Jenison MC, Saeland S, Shlomchik WD, Shlomchik MJ. Epidermal langerhans cell-deficient mice develop enhanced contact hypersensitivity. Immunity. 2005; 23:611–620. [PubMed: 16356859]
50. Mallick-Wood CA, et al. Conservation of T cell receptor conformation in epidermal gamma delta cells with disrupted primary Vgamma gene usage. Science. 1998; 279:1729–33. [PubMed: 9497293]
51. Hara H, et al. Development of dendritic epidermal T cells with a skewed diversity of gamma delta TCRs in V delta 1-deficient mice. J Immunol. 2000; 165:3695–705. [PubMed: 11034374]
52. Oettgen HC, et al. Active anaphylaxis in IgE-deficient mice. Nature. 1994; 370:367–370. [PubMed: 8047141]
53. Dombrowicz D, Flamand V, Brigman KK, Koller BH, Kinet JP. Abolition of anaphylaxis by targeted disruption of the high affinity immunoglobulin E receptor alpha chain gene. Cell. 1993; 75:969–976. [PubMed: 8252632]
54. Feyerabend TB, et al. Cre-mediated cell ablation contests mast cell contribution in models of antibody- and T cell-mediated autoimmunity. Immunity. 2011; 35:832–844. [PubMed: 22101159]
55. Barnden MJ, Allison J, Heath WR, Carbone FR. Defective TCR expression in transgenic mice constructed using cDNA-based alpha- and beta-chain genes under the control of heterologous regulatory elements. Immunol Cell Biol. 1998; 76:34–40. [PubMed: 9553774]
56. Mombaerts P, Clarke AR, Hooper ML, Tonegawa S. Creation of a large genomic deletion at the T-cell antigen receptor beta-subunit locus in mouse embryonic stem cells by gene targeting. Proc Natl Acad Sci U S A. 1991; 88:3084–7. [PubMed: 1826563]
57. Rickert RC, Roes J, Rajewsky K. B lymphocyte-specific, Cre-mediated mutagenesis in mice. Nucleic Acids Res. 1997; 25:1317–1318. [PubMed: 9092650]
58. Hollister K, et al. Insights into the role of Bcl6 in follicular Th cells using a new conditional mutant mouse model. J Immunol. 2013; 191:3705–3711. [PubMed: 23980208]
59. Workman P, et al. Guidelines for the welfare and use of animals in cancer research. Br J Cancer. 2010; 102:1555–1577. [PubMed: 20502460]
60. Kilkenny C, Browne WJ, Cuthill IC, Emerson M, Altman DG. Improving bioscience research reporting: the ARRIVE guidelines for reporting animal research. PLoS Biol. 2010; 8:e1000412. [PubMed: 20613859]
61. Wu YC, Kipling D, Dunn-Walters D. Assessment of B Cell Repertoire in Humans. Methods Mol Biol. 2015; 1343:199–218. [PubMed: 26420719]
62. Hill MO. Diversity and Evenness: A Unifying Notation and Its Consequences. Ecology. 1973; 54:427–432.
63. Stern JN, et al. B cells populating the multiple sclerosis brain mature in the draining cervical lymph nodes. Sci Transl Med. 2014; 6 248ra107.
64. Martin VG, et al. Transitional B Cells in Early Human B Cell Development - Time to Revisit the Paradigm? Frontiers in immunology. 2016; 7:546. [PubMed: 27994589]

Europe PMC Funders Author Manuscripts

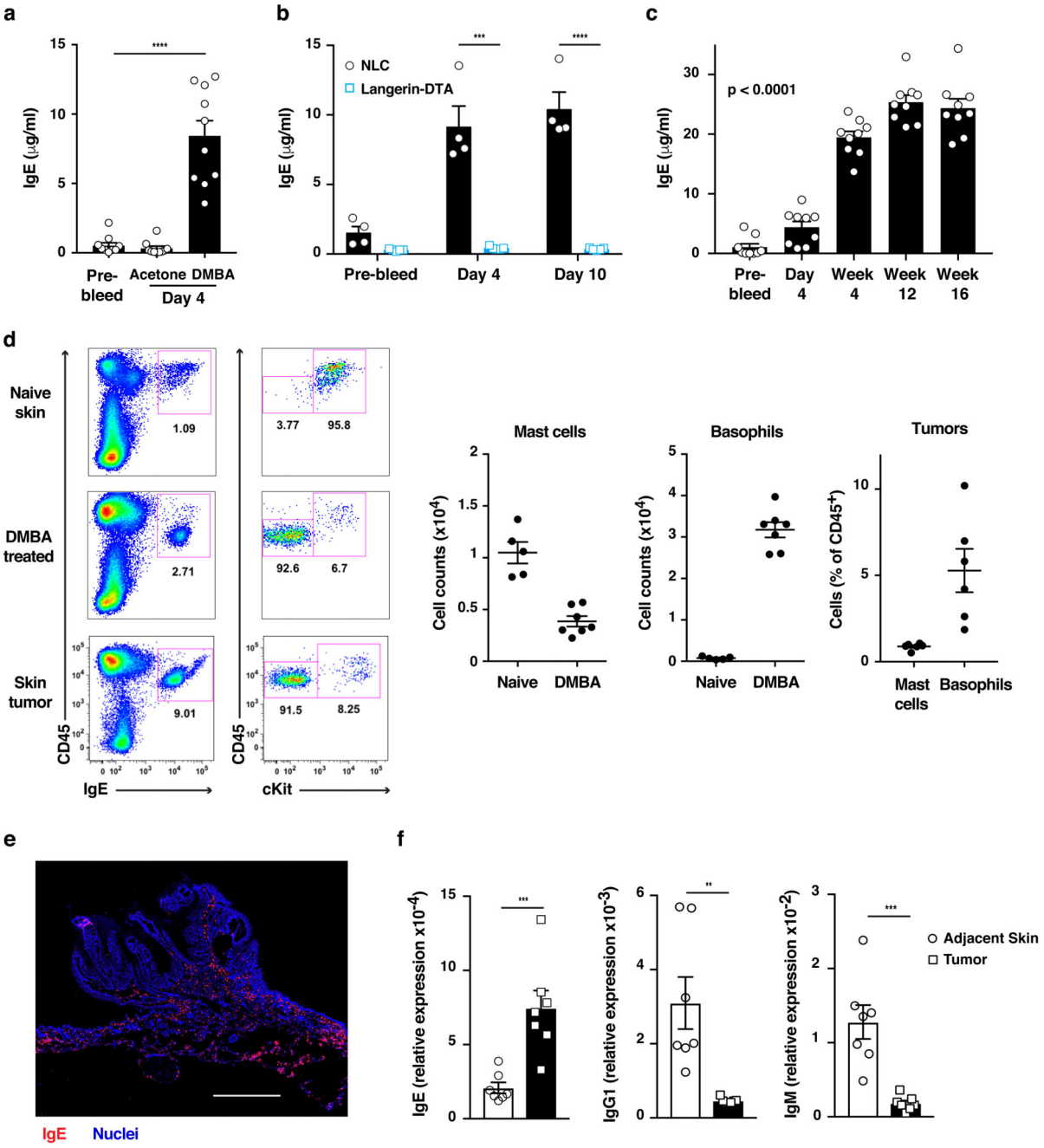

Figure 1. Carcinogen-induced epithelial cell damage triggers a rapid local and systemic IgE response

(a-c) ELISA of IgE in serum of (a) wild-type FVB mice treated with a single topical dose of 200nmol DMBA or vehicle control (acetone) on shaved back skin (n=10), (b) Langerin-DTA mice (n=5) and their non-transgenic littermate controls (NLC) (n=4) exposed to DMBA as in (a), (c) wild-type FVB mice exposed topically to 200nmol DMBA once weekly (n=9/group). Sera were analyzed for IgE at indicated time points and data expressed as mean ± SEM. (d) FACS analysis of IgE-bearing cells in naïve skin, DMBA-treated skin 7 days after exposure and in DMBA-induced skin tumors. Mast cells were defined as $CD45^{hi}cKit^{+}IgE^{+}$

Europe PMC Funders Author Manuscripts

and basophils as $CD45^{lo}cKit^{-}IgE^{+}$. Representative flow plots and enumeration shown (n=5 naïve skin, n=7 DMBA skin, n=6 tumors). (e) Representative image of IgE staining (red) in a DMBA-induced tumor. Nuclei in blue. Scale = 1mm. Image is representative of tile-scans from 6 independent tumors. (f) Quantitative RT-PCR analysis of mature immunoglobulin transcripts in tumors or tumor adjacent skin following DMBA carcinogenesis. Data are expressed as mean ± SEM relative to the control gene cyclophylin (n=7/group). Statistics using two-tailed unpaired Student's t-test (a and f), multiple t-tests (b) or one-way ANOVA testing for linear trend of IgE increase with time (c); **p<0.01, ***p<0.001 and ****p<0.0001. Data are representative of 3 (a,c,f), 2 (b) or 4 (d) independent experiments with similar results.

Europe PMC Funders Author Manuscripts

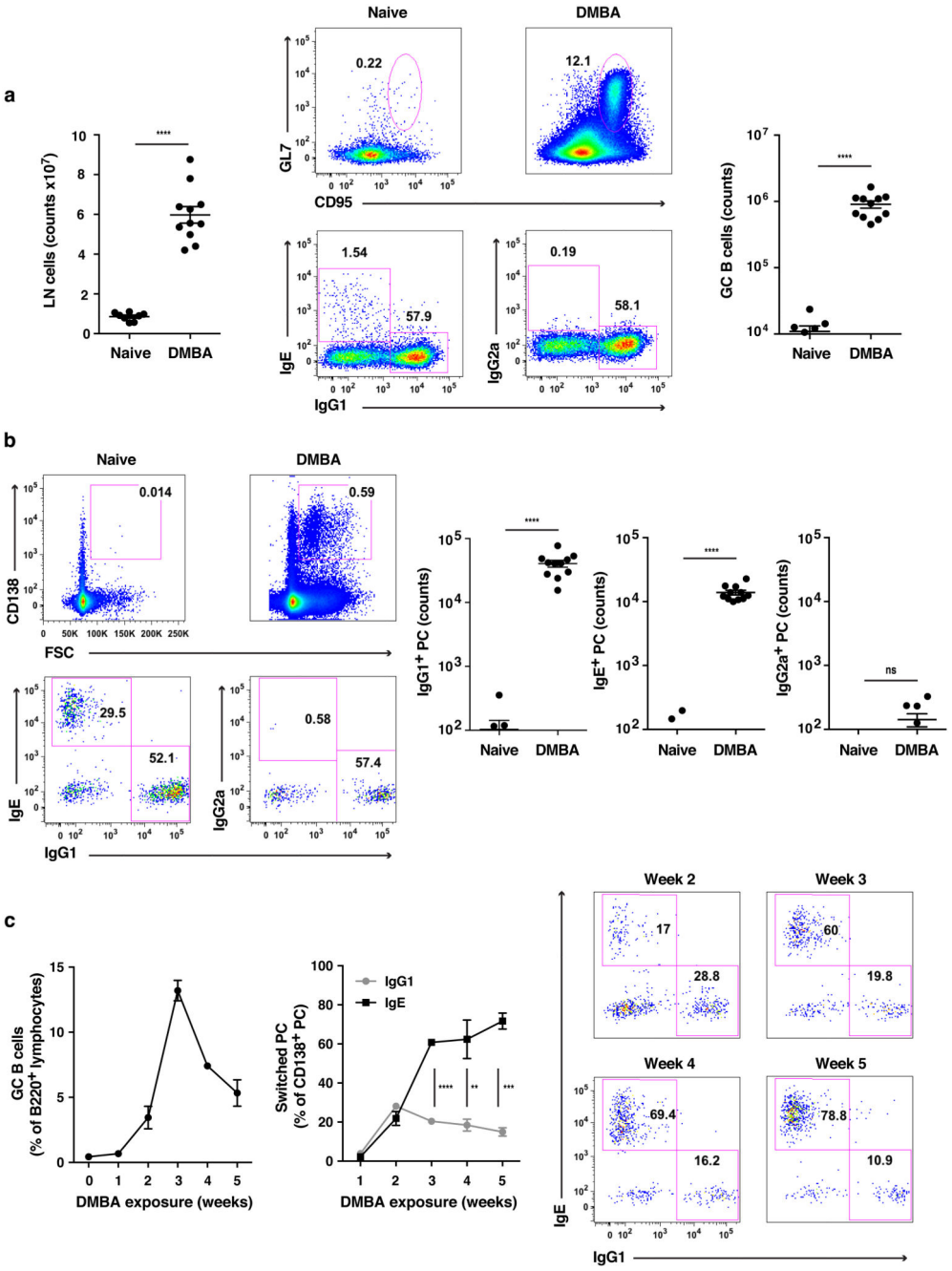

Figure 2. Topical carcinogen exposure induces local B cell class-switching resulting in a dominant IgE response

(a-c) FACS analysis of humoral immunity in the skin draining LNs of (a-b) wild-type FVB mice exposed topically to DMBA on the dorsal side of the ears twice, 3 days apart, and analyzed 7 days after last exposure and (c) wild-type FVB mice exposed to DMBA once weekly on shaved back skin and analysed 7 days after last exposure. (a) Total LN cells (left panel) and the number of GC B cells (right panel) defined as $B220^{+}CD95^{+}GL7^{+}$ LN cells were enumerated and compared to naïve wild-type mice. Representative flow plots show GC gated B cells and intracellular immunoglobulin staining to analyse GC B cell class-

switching. (b) Representative flow plots and enumeration of PCs, gated as $FSC^{hi}CD95^{+}CD138^{+}$ cells, and intracellular immunoglobulin staining to determine isotype switching. (a-b) naïve controls (n=9), DMBA treated (n=11). (c) The axillary LN B cell response was analyzed weekly at indicated time-points (n=3 per time-point). Statistical analysis by two-tailed Student's t-test for unpaired data; *p<0.05, ***p<0.001 and ****p<0.0001. ns = not significant. Data show one experiment representative of 5 (a,b) and 2 (c) independent experiments with similar results. Enumerated data are presented as mean ± SEM.

Europe PMC Funders Author Manuscripts

Europe PMC Funders Author Manuscripts

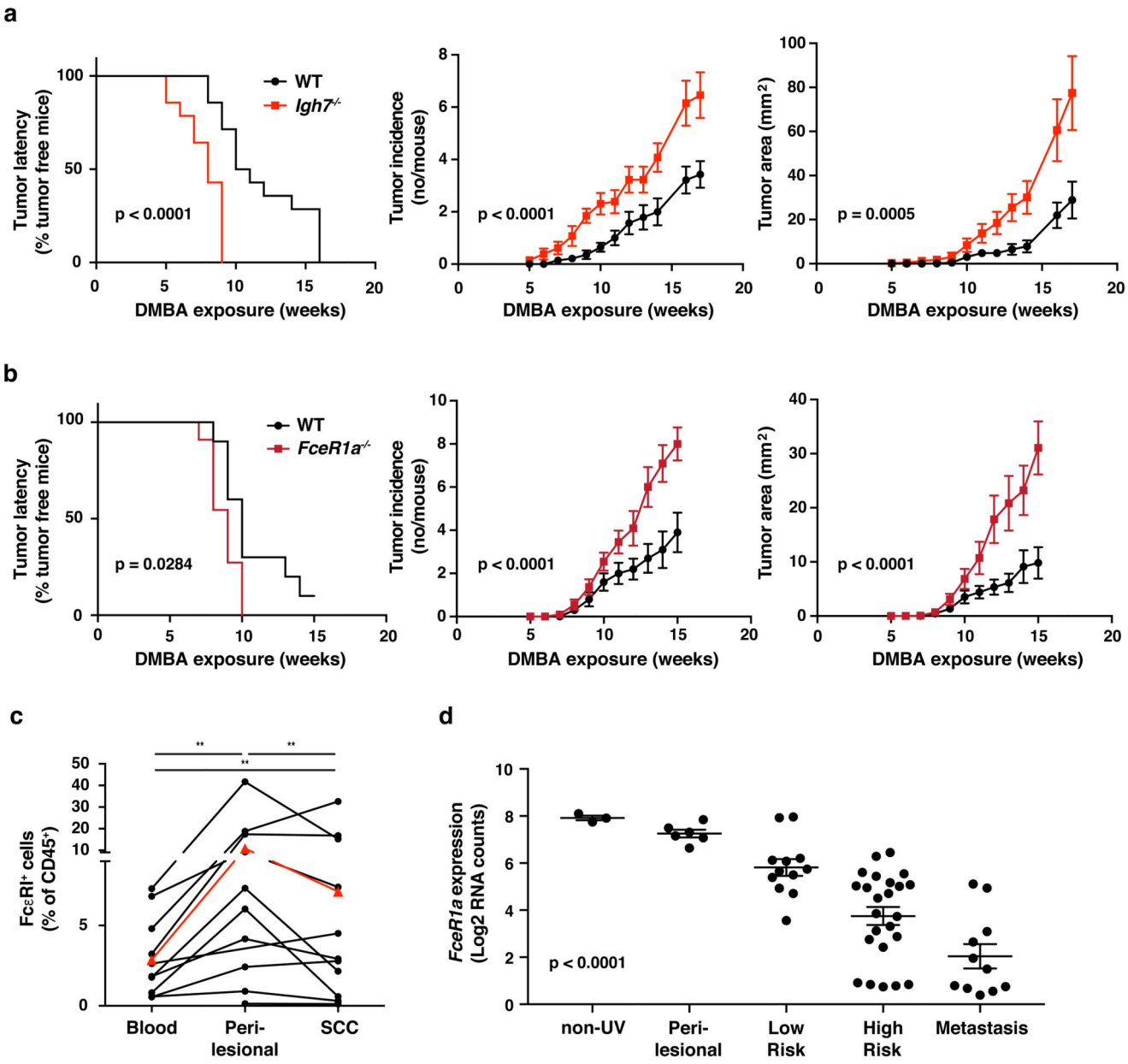

Figure 3. Carcinogen-induced IgE protects against carcinogenesis

(a-b) Tumor susceptibility expressed as tumor latency (time to appearance of first tumor), tumor incidence (average number of tumors per mouse) and tumor area (average tumor size per mouse) in (a) BALB/c wild-type and *Igh7*$^{-/-}$ mice (n=14/group) and (b) BALB/c wild-type (n=10) and *FceR1a*$^{-/-}$ (n=11) mice following DMBA-induced carcinogenesis. Data are expressed as mean ± SEM and statistical significance assessed using Log-rank (Mantel-Cox) test for tumor latency and linear regression for tumor incidence and area. (c) FACS analysis of FcεRI^{+} cells among total CD45^{+} leukocyte infiltrate in human SSC tissue, peri-lesional skin and matched blood samples (n=12 for SSC and n=10 for peri-lesional skin and blood). Red triangles depict mean proportion of FcεRI^{+} cells in the group. Statistical analysis by

paired Wilcoxon test; **p<0.01. (d) Tissue transcripts of *FceR1a* in whole human skin and SSC tissue were analyzed by NanoString nCounter. The tissue was collected and scored independently for 'tumor risk' by an experienced dermatopathologist; non-UV (n=3), peri-lesional (n=6), low risk SSC (n=12), high risk SSC (n=24) and metastasis (n=11). Log2 RNA counts of FcεRI are shown for individual 'risk groups' and presented as mean ± SEM. Statistics using one-way ANOVA and testing for linear trend of expression between 'risk groups'. Data in (a,b) are representative of 2 independent experiments with similar results. WT = wild-type.

Europe PMC Funders Author Manuscripts

Europe PMC Funders Author Manuscripts

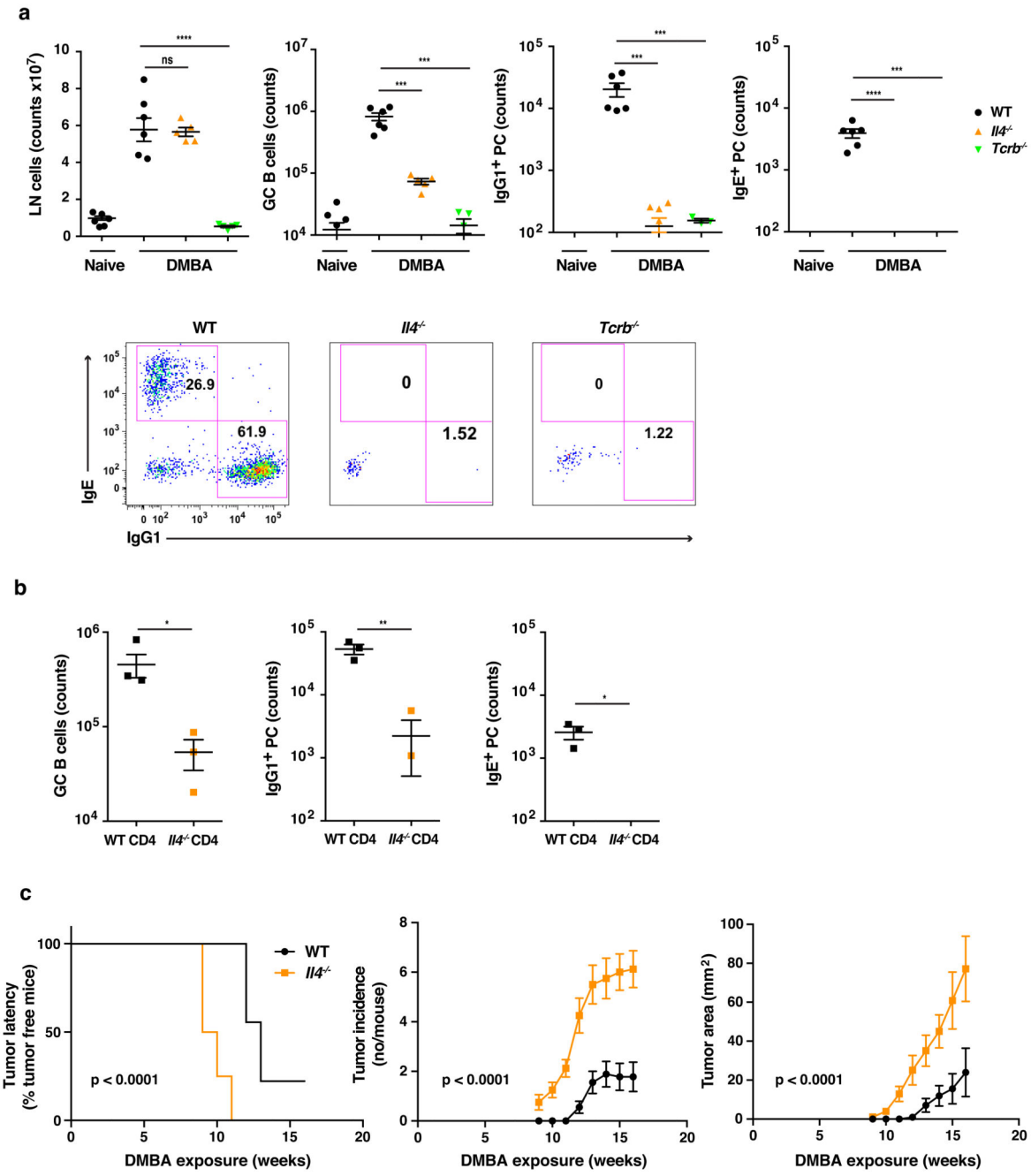

Figure 4. Carcinogen-induced humoral immunity depends on αβ T cell-derived IL-4

(a) FACS analysis of humoral immunity in the skin draining LNs of FVB wild-type (n=6), *Il4*$^{-/-}$ (n=5) and *Tcrb*$^{-/-}$ (n=5) mice exposed topically to DMBA on the dorsal side of the ears twice, 3 days apart, and analysed 7 days after the last exposure relative naïve wild-type controls (n=6). Graphs show number of total LN cells, B220^{+}CD95^{+}GL7^{+} GC B cells and IgG1^{+} or IgE^{+} FSC^{hi}CD95^{+}CD138^{+} PCs presented as mean ± SEM. Representative flow plots show IgG1^{+} and IgE^{+} PCs in wild-type, *Il4*$^{-/-}$ and *Tcrb*$^{-/-}$ mice. (b) FACS analysis of humoral immunity in the skin draining LNs of *Tcrb*$^{-/-}$ mice reconstituted with wild-type

Europe PMC Funders Author Manuscripts

$CD4^+$ αβ T cells (n=3) or *Il4*$^{-/-}$ $CD4^+$ αβ T cells (n=4) 1 day prior to topical DMBA exposure as described in (a). Statistics in (a-b) by two-tailed Student's t-test for unpaired data; *p<0.05, **p<0.01, ***p<0.001 and ****p<0.0001. ns = not significant. (c) Tumor susceptibility expressed as tumor latency (time to appearance of first tumor), tumor incidence (average number of tumors per mouse) and tumor area (average tumor size per mouse) in FVB wild-type and *Il4*$^{-/-}$ mice (n=9/group) following DMBA-induced carcinogenesis. Data are expressed as mean ± SEM and statistical significance assessed using Log-rank (Mantel-Cox) test for tumor latency and linear regression for tumor incidence and area. Data in (a,b) are representative of 3 independent experiments with similar results. WT = wild-type.

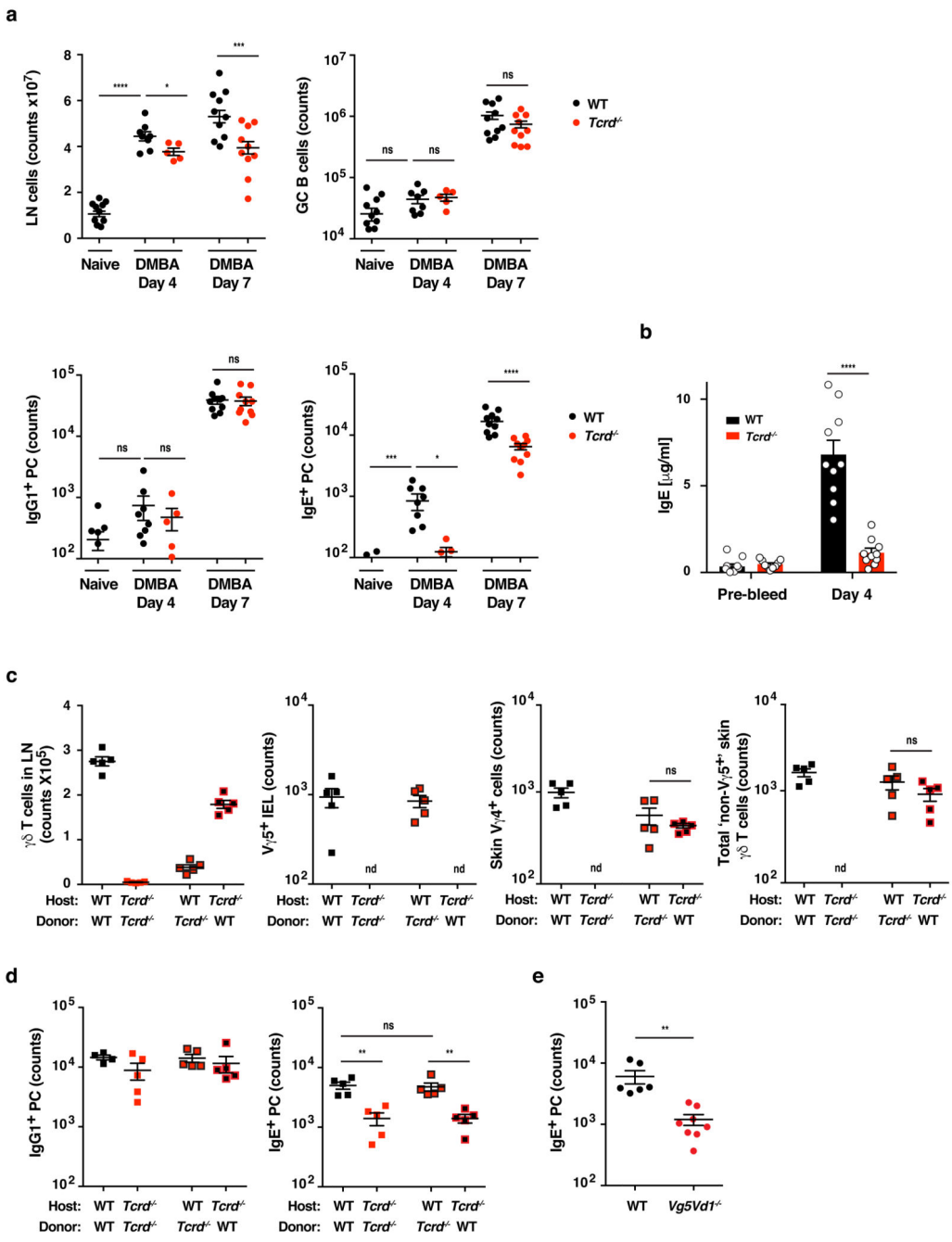

Figure 5. Induction of tumor-protective IgE requires γδ TCR$^+$ IEL

(a) FACS analysis of humoral immunity in the skin draining LNs of FVB wild-type and *Tcrd*$^{-/-}$ mice exposed topically to DMBA on the dorsal side of the ears twice, 3 days apart, and analyzed 4 or 7 days after last exposure (wild-type naïve (n=10), wild-type 4 days (n=8), wild-type 7 days (n=10), *Tcrd*$^{-/-}$ 4 days (n=5), *Tcrd*$^{-/-}$ 7 days (n=10)). Graphs show number of total LN cells, B220$^+$CD95$^+$GL7$^+$ GC B cells and IgG1$^+$ or IgE$^+$ FSC^{hi}CD95$^+$CD138$^+$ PCs. (b) ELISA of IgE in serum of wild-type and *Tcrd*$^{-/-}$ mice topically exposed to DMBA on shaved back skin and bled before and 4 days after exposure (n=10/group). (c-d) FACS

analysis and enumeration of (c) LN and skin γδ T cells and (d) humoral immunity in the skin draining LNs of *Tcrd*$^{-/-}$→wild-type and wild-type→*Tcrd*$^{-/-}$ chimeric mice relative to chimeric control mice following exposure to DMBA and analysis at day 7 as in (a) (n=5/group). (e) FACS analysis of IgE^{+} PCs in the skin draining LNs of FVB wild-type (n=6) and *Vg5Vd1*$^{-/-}$ (n=8) mice exposed to DMBA and analysed as in (a). Statistics in (a-d) by one-way ANOVA multiple comparison and (e) two-tailed Student's t-test for unpaired data; *p<0.05, **p<0.01, ***p<0.001 and ****p<0.0001. ns = not significant. nd = not detected. All data presented as mean ± SEM. Data show one experiment representative of 3 (a,b) and 2 (c,d) independent experiments with similar results. WT = wild-type.

Europe PMC Funders Author Manuscripts

Europe PMC Funders Author Manuscripts

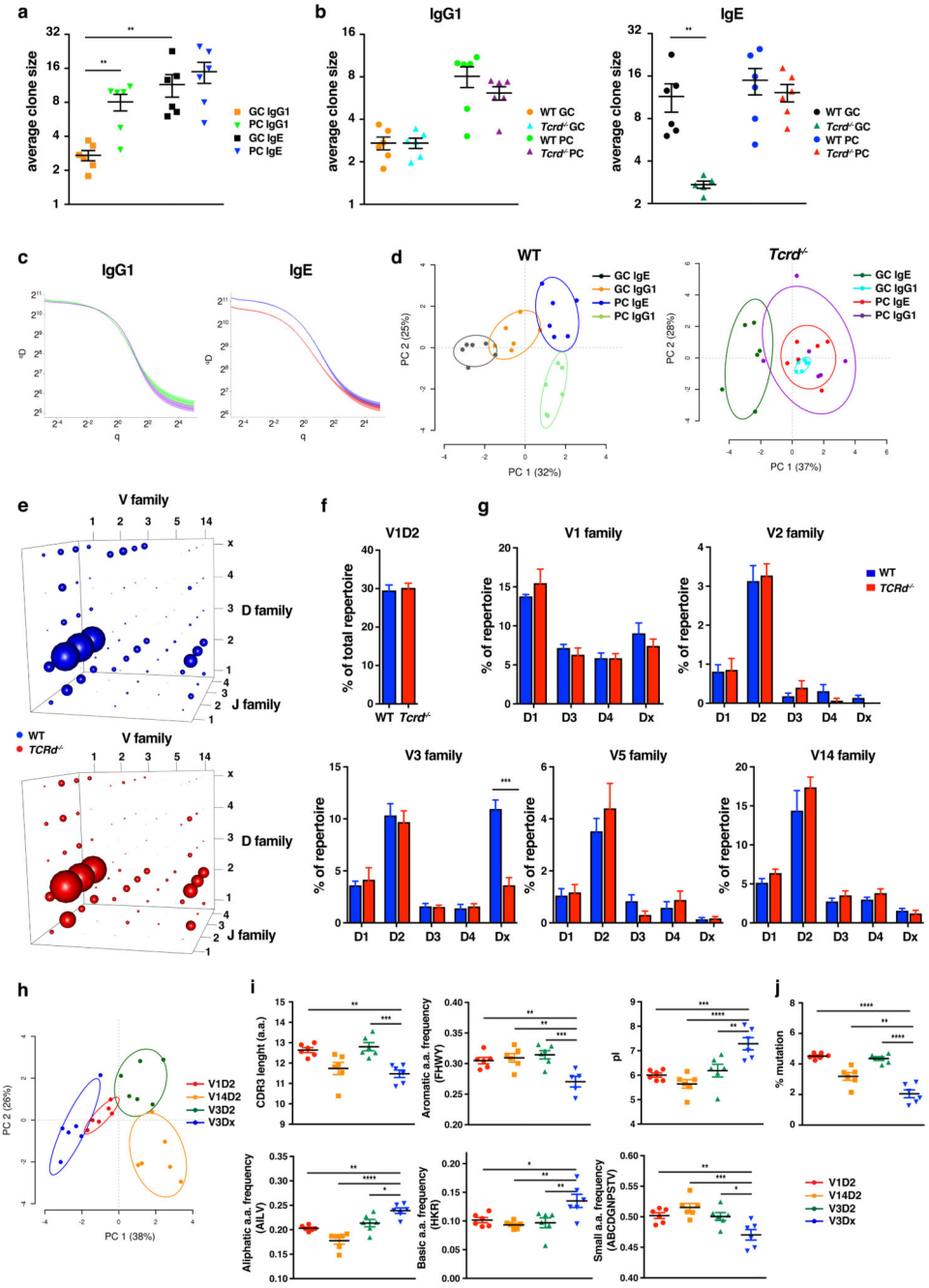

Figure 6. γδ T cells promote a distinct IgE repertoire in response to carcinogen

(a-j) High-throughput sequencing and heavy-chain repertoire analysis of IgG1 and IgE in sorted B220^{+}CD95^{+}GL7^{+} GC B cells and FSC^{hi}CD95^{hi}CD138^{+} PCs from skin draining LNs of wild-type and *Tcrd*$^{-/-}$ mice 7 days after the last of two topical exposures to DMBA (n=6/group). (a-b) Average clone size. (c) Average clonal diversity of IgG1 and IgE PC repertoires in wild-type and *Tcrd*$^{-/-}$ mice ('General diversity index (^{q}D)' displayed as a measure of 'clonal frequencies (q)'; $p<0.05$ for IgE from $q<2^{2}$). (d) Kidera factor PCA showing IgG1^{+} and IgE^{+} GC B cells and PCs in wild-type (left) and *Tcrd*$^{-/-}$ mice (right). (e)

3D plot of average VDJ gene family usage in IgE^+ PCs in wild-type (top) versus *Tcrd*$^{+/-}$ (bottom) mice. V and D genes used <1% in the repertoire removed for clarity. (f-g) VD repertoire of IgE^+ PCs in wild-type and *Tcrd*$^{+/-}$ mice with (f) showing % use of V1D2 and (g) % use of other VD combinations after V1D2 exclusion. (h) Kidera factor PCA, (i) CDRH3 length and indicated characteristics and (j) % mutations in CDRH3 compared to germline in V3Dx clones compared to other indicated VD families in wild-type IgE^+ PCs. Statistics by two-tailed Student's t-test for unpaired data (a, b, f and g) and one-way ANOVA multiple comparison (i-j); *p<0.05, **p<0.01, ***p<0.001 and ****p<0.0001. Data in a,b,f,g,i presented as mean ± SEM. WT = wild-type.

Europe PMC Funders Author Manuscripts

Europe PMC Funders Author Manuscripts

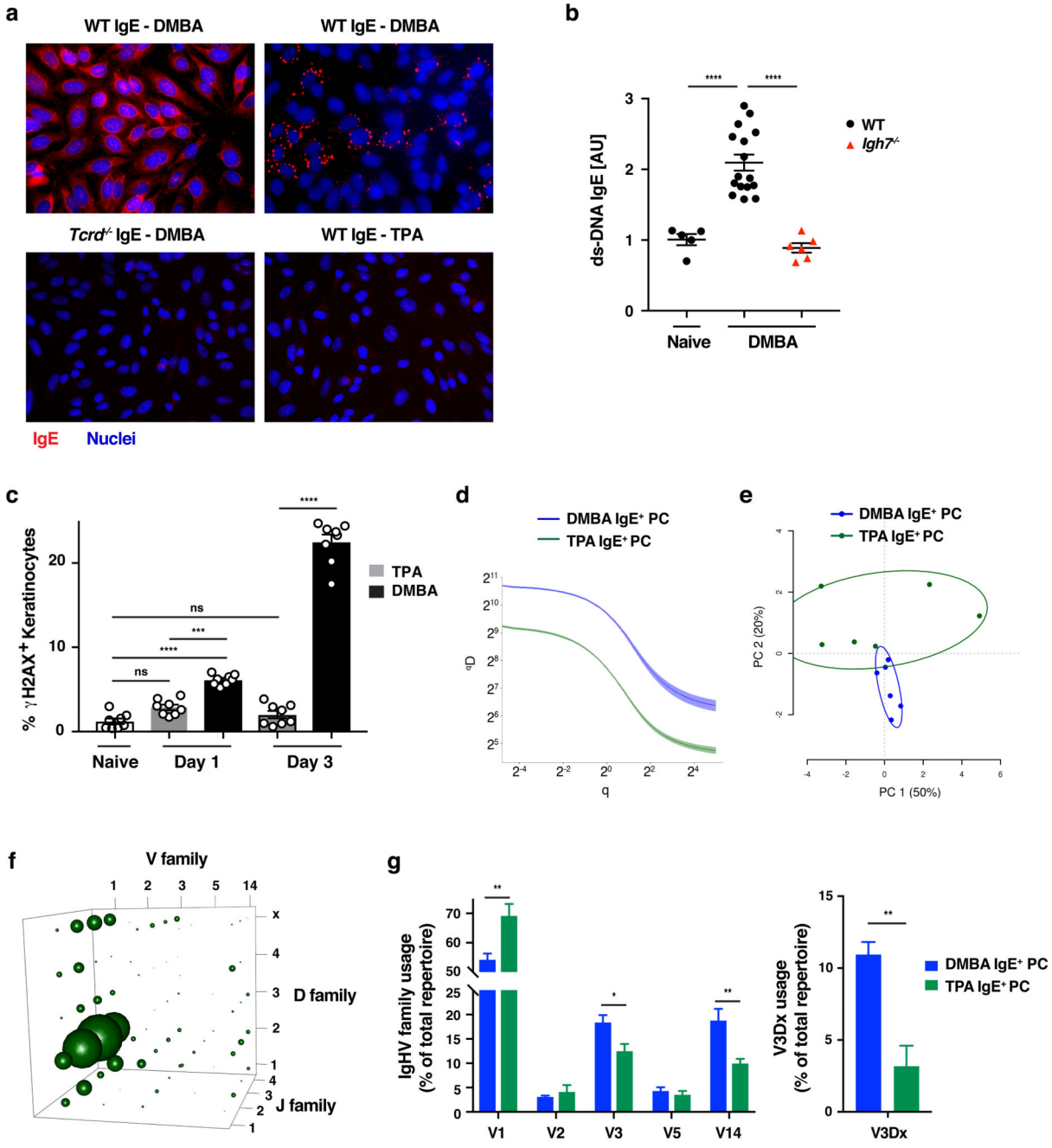

Figure 7. DMBA-induced IgE is autoantigenic and differs from TPA-induced IgE

(a) Autoreactive binding to HEp-2 cells of IgE in serum from DMBA-treated wild-type or *Tcrd*$^{-/-}$ mice and TPA-treated wild-type mice (serum diluted 1:25, 1:5 and 1:5 respectively to match IgE titers). Examples of the most common patterns are shown, IgE binding (red) and nuclei (blue). (b) ELISA of anti-ds-DNA autoreactivity of IgE in serum from DMBA-treated wild-type (n=16) or *Igh7*$^{-/-}$ (n=6) mice and naïve wild-type controls (n=5). (c) FACS analysis of γH2AX expression in CD45^{-} skin epithelial cells, as a measure of ds-DNA breaks, at indicated time-points after topical DMBA or TPA (n=8/group). (d-g) High-

throughput sequencing and heavy-chain repertoire analysis of IgE in sorted $FSC^{hi}CD95^{hi}CD138^{+}$ PCs from skin draining LNs of wild-type mice 7 days after topical exposures to DMBA or TPA (n=6/group). (d) Average clonal diversity throughout the IgE^{+} PC repertoire ('General diversity index (^{q}D)' displayed as a measure of 'clonal frequencies (q)'; $p<0.05$ throughout the repertoire). (e) Kidera factor PCA showing CDRH3 properties, (f) 3D plot of average VDJ gene family usage in TPA-induced IgE and (g) use of the 5 most common V families as % of the total repertoire and frequency of the V3Dx clones after topical DMBA or TPA treatment. Statistics by one-way ANOVA multiple comparison (b and c) or two-tailed Student's t-test for unpaired data (g); *p<0.05, **p<0.01, ***p<0.001 and ****p<0.0001. ns = not significant. Data in b,c,g expressed as mean ± SEM. WT = wild-type.